

8<sup>th</sup> US National Combustion Meeting  
Organized by the Western States Section of the Combustion Institute  
and hosted by the University of Utah  
May 19-22, 2013.

## Direct Numerical Simulation of Autoignition of a Hydrogen Jet in a Preheated Cross Flow

*Ammar Abdilghanie*<sup>1</sup>      *Christos E. Frouzakis*<sup>2</sup>      *Paul Fischer*<sup>3</sup>

<sup>1</sup>*Leadership Computing Facility,  
Argonne National Laboratory, Argonne, IL 60439*

<sup>2</sup>*Aerothermochemistry and Combustion Systems Laboratory,  
Swiss Federal Institute of Technology Zurich (ETHZ), Zurich, Switzerland*

<sup>3</sup>*Mathematics and Computer Science Division,  
Argonne National Laboratory Argonne, IL 60439*

Autoignition of a nitrogen-diluted hydrogen mixture issuing from a round nozzle into a cross-flowing turbulent stream of preheated air flowing in a channel at a friction Reynolds number  $Re_\tau = 180$  is investigated via 3-D direct numerical simulations (DNS) at two crossflow stream temperatures (930 and 950 K). Three-dimensional visualizations of the JICF reveal a complicated flow structure characterized by a variety of coherent vortical structures resulting from the boundary layers near the walls and evolving from the jet instabilities. The mean pressure field set up by the flow continuously drives the cross-flow fluid into the jet on the downstream side leading to enhanced entrainment relative to the upstream side and jet asymmetry. Autoignition of the jet depends sensitively on the cross-flow temperature. At the highest studied cross-flow temperature, spatially-isolated flame kernels form downstream of the jet, early on in the simulation. Although such flame kernels tend to propagate upstream, they get convected out of the domain. Later on, a strongly burning flame forms near the jet nozzle. At the lower cross-flow temperature, similar dynamics are observed significantly later in time and farther downstream from the nozzle.

### 1 Introduction

Understanding the conditions under which reacting mixtures autoignite is of primary importance for the design and operation of modern lean premixed (LP) and lean premixed prevaporized (LPP) combustion devices such as low- $\text{NO}_x$  stationary gas turbines [1] and propulsion devices such as subsonic ramjets and supersonic scramjets [2]. In particular, the enhanced turbulent mixing between the fuel and oxidizer streams of the jet in cross flow (JICF) configuration makes it an essential component in the design of premixing sections of modern high efficiency, low  $\text{NO}_x$  combustors.

The non-reacting JICF is characterized by vortical structures which result from distinct physical processes and lead to rich fluid dynamics [3]. Four types of coherent structures are typically found in a JICF: (i) counter-rotating vortex pair (CVP) downstream of the jet as a result of accumulation of its azimuthal vorticity in the direction of the deflected jet trajectory [4], (ii) shear layer vortices resulting from inviscid/Kelvin-Helmholtz instability of the jet flow, (iii) wake vortices (WVs) behind the jet and (iv) horse-shoe vortices (HSV) close to the wall both upstream and downstream

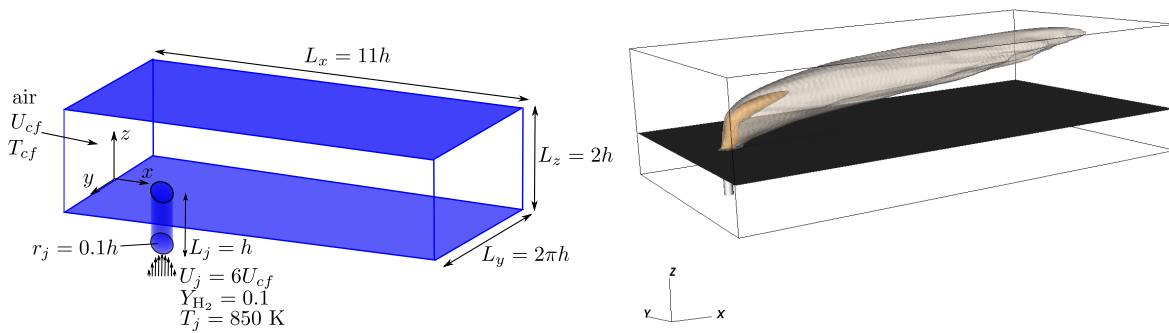


**Figure 1: Left: schematic of the geometry and the computational domain. Right: isosurfaces of the mean mixture fraction at the stoichiometric (inner isosurface) and most reactive (outer isosurface) values for the  $T_{cf} = 930$  K case.**

of the jet nozzle. The dynamics of the non-reactive JICF are thus associated with fast time-scales (shear layer vortices), intermediate (CVP) and slow time-scales (WVs) [5]. Most of the previous non-reactive JICF studies focused on the scaling laws of the velocity and scalar concentration fields, fitting the jet trajectory and its penetration into the cross flowing stream [6–8].

Through experimental observations, Hasselbrink et al. [9] found that a methane JICF penetrates slightly deeper into the cross flow leading to measurable, albeit small, deviation of the jet trajectory relative to a chemically-inert JICF. They also suggested that heat release can possibly affect the rate of entrainment of the cross-flowing fluid. More recently, Feck et al. [10] compared experimentally estimated ignition delay times (denoted by the emergence of flame kernels leading to stabilized flames) to the computed ignition delay times in homogeneous reactors at different operating pressures (5, 10 and 15 bar). It was found that low cross-flow temperatures inhibit ignition while pressure does not have a noticeable impact on ignition especially at low cross-flow velocities. The experimentally estimated ignition delay times were significantly shorter than the minimum delay times in homogeneous systems suggesting that turbulent mixing and flow inhomogeneity can significantly alter the ignition behavior in the JICF configuration.

On the computational side, Grout et al. [11] investigated the stabilization mechanism of a transverse hydrogen jet in a hot cross flow of air using DNS. They found that the jet stabilizes in a low velocity region in the jet wake where the mixture fraction is stoichiometric. The alignment of the fuel and oxidant gradient, as quantified by the Takeno flame index [12], and the coexistence of large heat release suggested that the observed flame is a premixed deflagration wave. In their more recent work Grout et al. [5] introduced a smoothly varying jet path parameter based on the solution of a Laplace equation over and within a constant mixture fraction surface delineating the outer edges of the jet. In the jet parameter coordinate, they found a correlation between the flame base and a low velocity high enstrophy region. Unlike the test section of the experimental setup of Feck et al. [10], in [5, 11] the cross-flowing stream is a boundary layer flow with no vertical confinement. It is thus of interest to understand the behavior of a jet in cross-flowing turbulent channel flow both as a fundamentally different problem and also as a more relevant prototype for a subclass of practical applications.

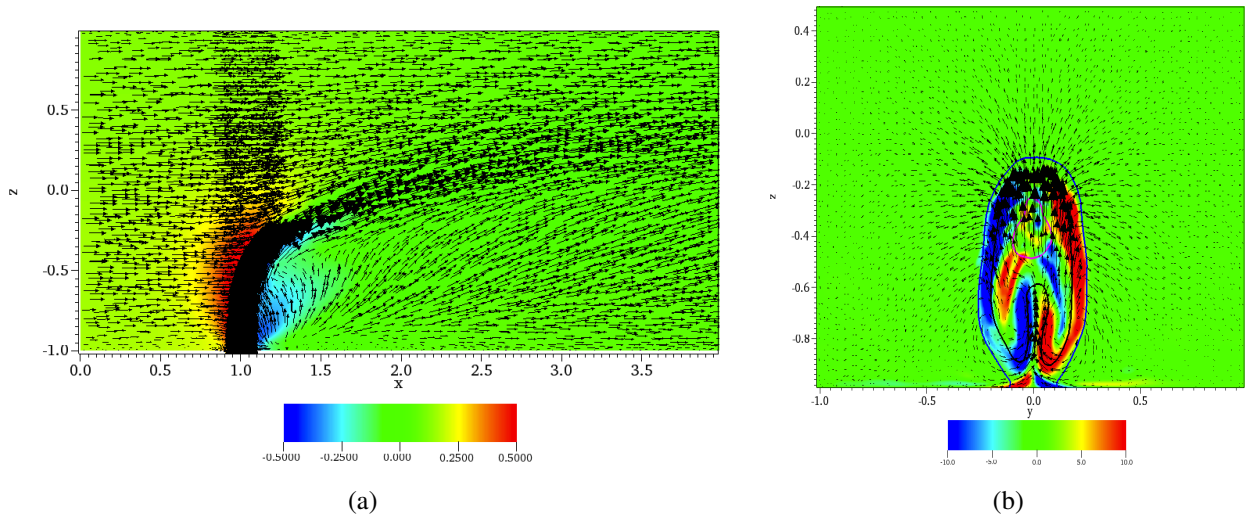


**Figure 2: (a) Mean kinematic pressure distribution over a mid spanwise ( $xz$ ) plane ( $y = 0$ ) for the  $T_{cf} = 930$  K case with velocity vector plots. (b) Mean stream wise vorticity component over a transverse ( $yz$ ) plane at  $x = 1.25$ . In (b), three mixture fraction isolines are overlaid; the most reactive ( $\xi_{MR} = 0.03$  in blue), the stoichiometric ( $\xi_{st} = 0.226$  in black) and ( $\xi = 0.5$  in pink).**

The main objective of this study is to investigate the sensitivity of autoignition and the long-term JICF dynamics to the cross-flow temperature. The focus is on the localization in space and time of the autoignition kernels and the relation of the ignition time to the ignition delay of a homogeneous mixture. With respect to the long-term behavior, the aim is to identify whether strongly-burning flames will be established from the ignition kernels as well as about the local combustion mode associated with the kernels.

## 2 Mathematical formulation and computational domain description

The compressible reactive Navier-Stokes of an ideal gas mixture in the low Mach number limit were solved using a parallel code based on the incompressible spectral element solver nek5000 [13]. The spectral element method is a high-order weighted residual technique that couples the rapid convergence of global spectral methods with the geometric flexibility of finite element methods [14].

A high-order operator splitting technique is used to split the thermochemistry (species and energy equations) from the hydrodynamic subsystem (continuity and momentum equations) [15]. The latter is integrated in time using a 3rd-order semi-implicit scheme, with explicit treatment of the nonlinear terms and implicit treatment of the viscous and pressure terms, while the thermochemistry subsystem is solved fully implicitly by CVODE, a scalable BDF-based stiff ODE solver [16]. Detailed chemistry, thermodynamic properties and mixture-averaged transport properties are evaluated using the Chemkin packages [17].

The computational domain (figure 1) consists of a channel with streamwise length (normalized by the channel half-height  $h = 1$  cm)  $L_x = 11$ , spanwise extent  $-\pi \leq y \leq \pi$  and height  $L_z = 2$  and a circular pipe centered at  $x = 1, y = 0, z = -1$  with length  $L_j = 1$  and radius

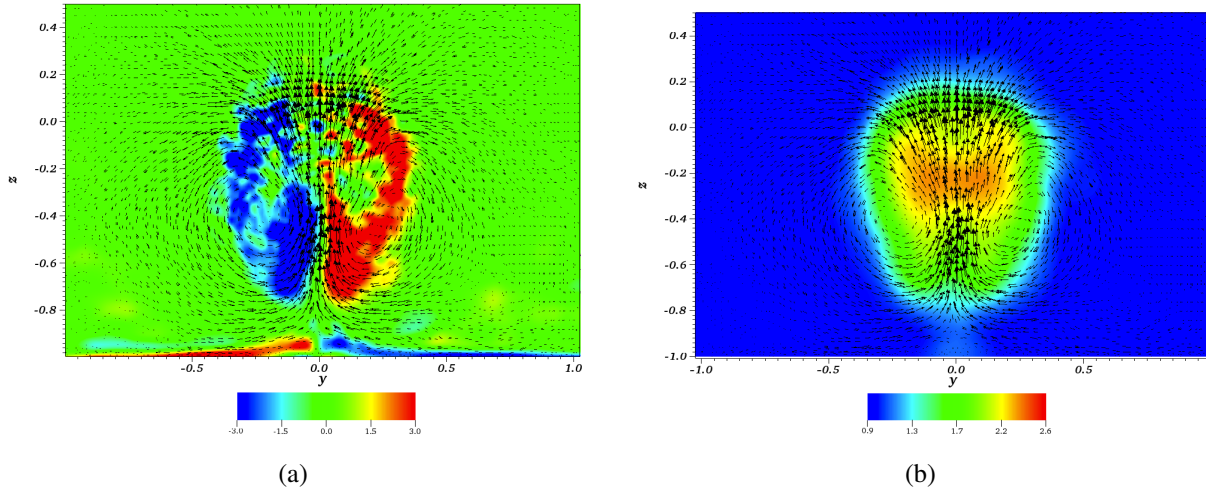


**Figure 3: Mean velocity vector plot on a transverse ( $yz$ ) plane at  $x = 2$  overlaid on (a) stream wise vorticity component (b) temperature for the  $T_{cf} = 930$  K.**

$r_j = 0.1$  with its discharge nozzle flush with the channel floor. The reference values used for non-dimensionalization are the bulk cross-flow velocity  $U_{cf} = 30.28$  m/s, the temperature  $T_{cf}$  and the properties of air at the inflow conditions; the reference time is  $t_{ref} = h/U_{cf} = 0.33$  ms.

The domain is discretized into 1,591,752 hexahedral elements. A square patch ( $0.6 \leq x \leq 1.4$  and  $-0.6 \leq y \leq 0.4$ ) is used to accommodate the jet and the region  $0.6 \leq x \leq 11$ ,  $-2 \leq y \leq 2$  is uniformly resolved with  $\delta x = \delta y = 0.4$ . In the vertical  $z$ -direction a tanh mapping is used to cluster the grid resolution close to the channel walls. The solution is obtained in terms of 5<sup>th</sup>-order Lagrange polynomials (six discretization points in each spatial direction and spectral element). The integration time step is set to  $10^{-4}$ .

An auxiliary DNS of the turbulent non-reactive flow in a channel was performed to create the initial velocity profile inside the channel as well as a database for the turbulent inflow which is interrogated during the simulation to obtain the turbulent inflow velocity profiles. The pipe is initially filled with quiescent air at the cross-flow stream temperature. For the cases reported here, the bulk Reynolds number based on the mean center line velocity and the half channel height is  $Re_b = 2800$ , corresponding to a friction Reynolds number of  $Re_\tau = 180$ . The remaining velocity boundary conditions are periodic in the spanwise direction, no-slip on the top and bottom walls and outflow (zero gradient) at the exit plane. The pipe inflow is laminar with a specified parabolic velocity profile injecting the fuel (10% hydrogen in nitrogen per mass) having a temperature of  $T_j = 850$  K; the jet to cross-flow velocity ratio is  $R_j = U_j/U_{cf} = 6$ . The cross-flowing fluid is air having a temperature of  $T_{cf} = 930$  K and 950 K in the two reported simulations. The walls and lateral surface of the pipe are considered as adiabatic with zero-flux boundary conditions for the species; zero Neumann boundary conditions are imposed at the outflow plane.

### 3 Results

The relatively high jet-to-cross-flow velocity ratio leads to the jet acting as a bluff body to the cross-flow and as a result a reduced pressure region (see figure 2(a)) forms on the downstream

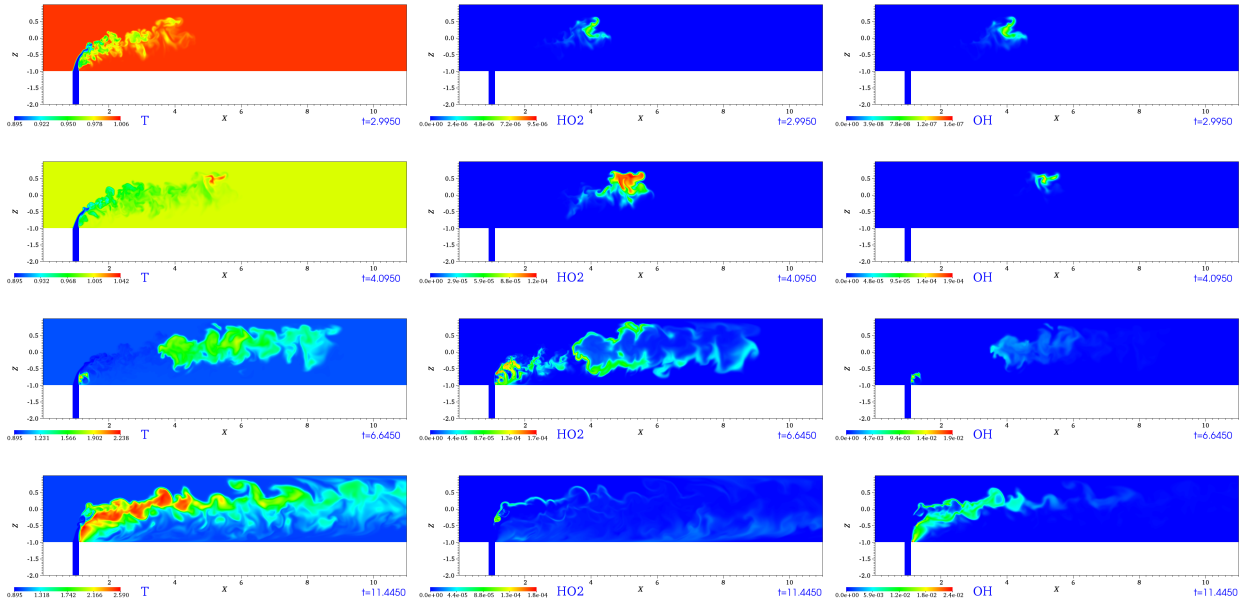


**Figure 4: Snapshots of mass fractions of  $\text{HO}_2$ ,  $\text{OH}$  and of temperature for the  $T_{cf} = 950$  K case**

side of the jet that appears to push cross-flow fluid towards the jet. Figure 2(a) also shows what may be considered as a source/node at  $x \approx 1.25$ ,  $z = -0.8$  from which the cross-flow seems to emanate [18], which acts to further enhance cross-flow entrainment on the downstream side of the jet leading to the noticeable asymmetry in figure 1. A transverse plane at the streamwise location of the node shows a converging cross-flow motion towards the node on the mid spanwise plane ( $y = 0$ ) and an upwelling motion that drives it further upwards towards the jet core. Two oppositely-signed large scale vortices are also seen on the transverse plane (Figure 2(b)) that appear to be early precursors of a more distinct CVP forming further downstream (see figure 3 (a)) and act to replenish the jet core (see figure 3(b)) with cross-flow fluid. The variation of the pressure field across the jet leads to deformation of the initially circular mixture fraction field near the inlet nozzle (figure 5(a), (b)) to a characteristic kidney-shaped cross section [18].

The reaction starts as soon as the fuel enters the hot cross flow. Hydroperoxy radicals form first at the tip of the fuel jet as it mixes with air. For  $T_{cf} = 950$  K, the first ignition kernel appears at  $t \approx 4$ , close to  $x \approx 5.2$ ,  $z \approx 0.5$  on the midplane of the domain. New kernels continue to form around that location, but they are all convected downstream by the flow. At  $t \approx 6.55$  an ignition kernel forms in the recirculation zone behind the jet and establishes a strongly burning flame (figure 4).

A similar behavior is observed for  $T_{cf} = 930$  K, although it takes significantly longer both for the first ignition kernel to appear and for the kernel to form in the recirculation zone. Up to  $t \approx 19$ , the mixture reacts slowly and the heat released is low (the temperature inside remains below the domain 937.5 K). The first ignition kernel appears off the vertical midplane and close to the outflow ( $x \approx 9.5$ ).

The similar behavior of the two cases can also be inferred from the comparison of the time histories of the integral of the non-dimensional heat release rate (iHRR) over the whole domain for the two cases shown in figure 6. Multiple autoignition kernels form in regions where the local mixture

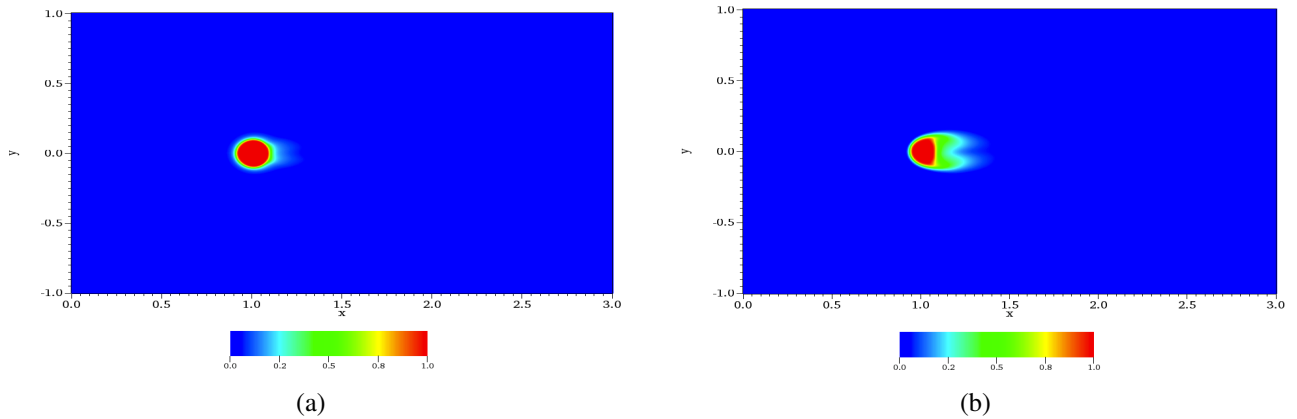


**Figure 5: Mean mixture fraction distribution over a horizontal ( $xy$ ) plane for the  $T_{cf} = 930$  K case, (a) at  $z=-1.0$ , (b)  $z=-0.9$ .**

fraction is equal to the most reactive mixture fraction value  $\xi_{MR}$  [19, 20]; i.e. the value associated with the minimum ignition delay time for the corresponding homogeneous system. They are all convected out of the domain until at  $t \approx 27.7$  the mixture ignites close to the nozzle axis but off the lower wall ( $z \approx -0.6$ ) and forms a strongly burning flame (figure 8(b)). The average taken over one flow-through time of the mid spanwise plane temperature field is shown in figure 8(c). Although it appears there is a single, strongly burning, spatially coherent reaction region, the instantaneous image (b) shows ensemble of broken reaction regions.

The most reactive mixture fraction estimated from the mixture with the minimum ignition delay time in a homogeneous constant pressure reactor is  $\xi_{MR} = 0.03$  for the  $T_{cf} = 930$  K case (assuming adiabatic mixing of the cross-flow and jet fluid as initial condition, figure 7) corresponding to an ignition delay time of  $\tau_{ign} = 3.1$  ms. For  $T_{cf} = 950$  K the  $\tau_{ign}$  curve has a very flat minimum of about 1 ms for mixture fraction values extending from 0.02 to 0.065.

Autoignition favors locations where the local velocity and mixing rate/scalar dissipation rate are low and the local temperature is relatively high as can be seen in the scatter plots of figure 9(1),(b) constructed from the mean data taken when the strongly-burning flame is established. The latter flame appears to be locally premixed as can be seen from the “white regions” in figure 10, where the gradients of the fuel and oxidizer are, on the mean, aligned. “Dark” regions where the fuel and oxidizer are negatively aligned appear to be on the upstream side of the jet and the far field and hence the flame on that side is mostly diffusion type. Investigation of multiple snapshots of the Takeno index distribution (not shown) over the same spanwise plane shows that the flame is composed of ensembles of locally premixed and non-premixed flame regions, however the premixed regions seem to dominate the downstream side local ignition mode.

## 4 Conclusions

Direct numerical simulation of a JICF configuration at two cross-flow temperatures are reported. It is seen that the JICF entrains more fluid on the downstream side by virtue of a combination of the existence of reduced pressure region behind the jet (which acts as an obstacle for high jet to cross-flow velocity ratios), and an efficient counter-rotating vortex (CVP) pair that pulls cross-flowing

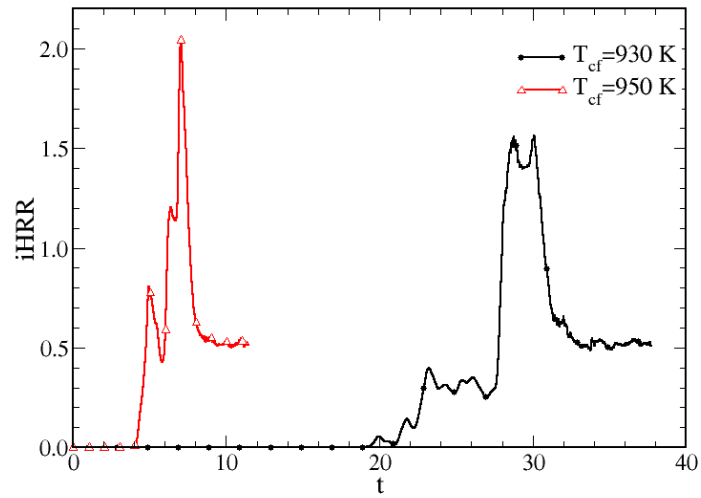


Figure 6: Time history of the total heat release rate normalized by its maximum value in the  $T_{cf} = 930$  K case.

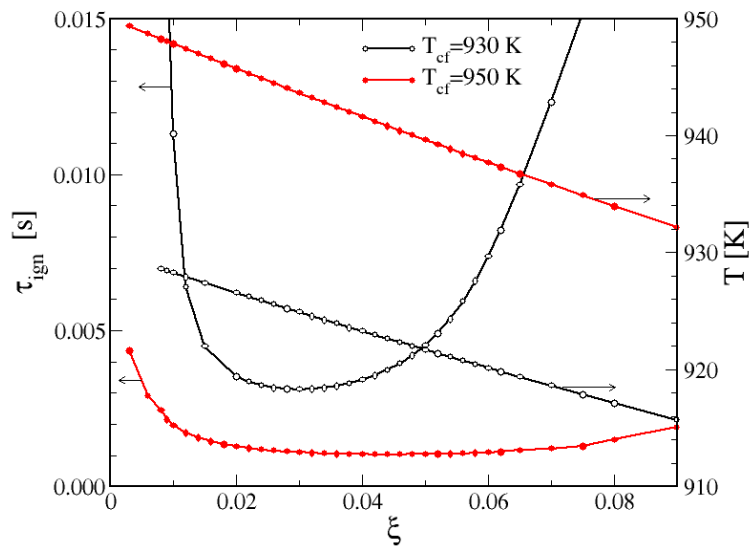
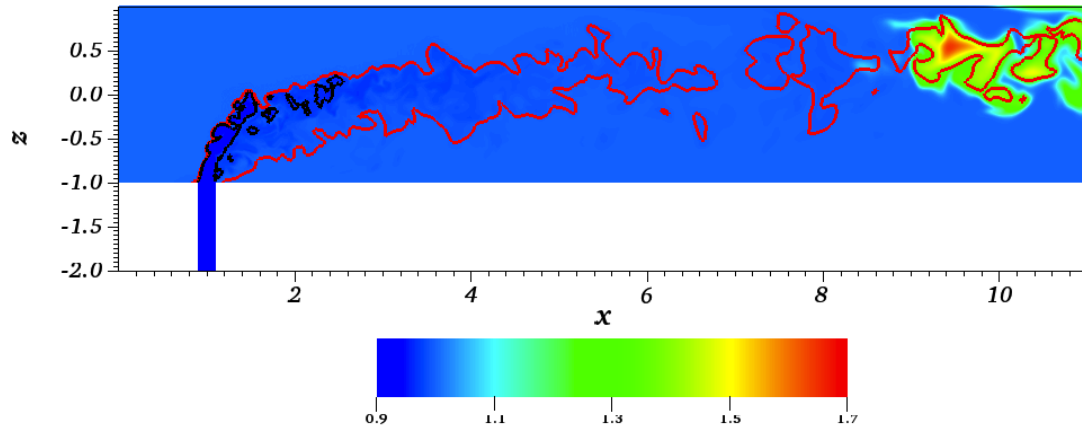
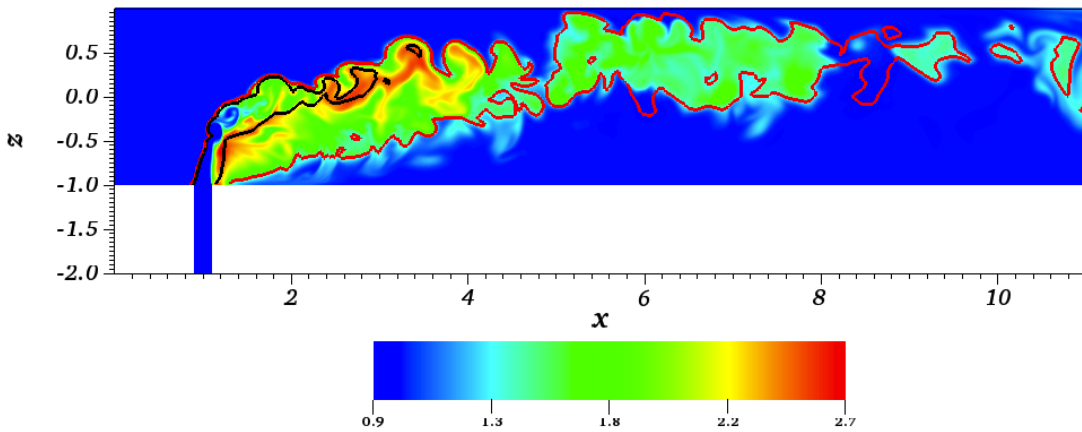


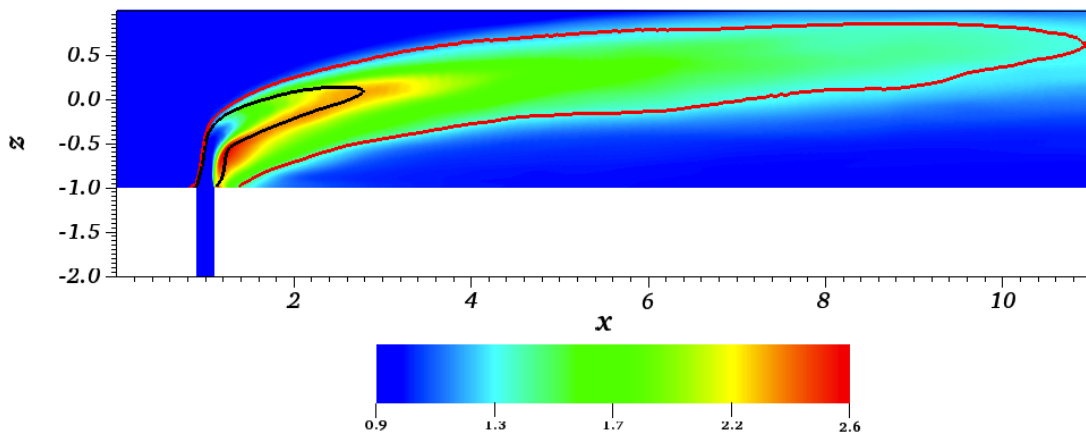
Figure 7: Ignition delay time of a homogeneous reactor for the  $T_{cf} = 930$  K (black line with open circles) and the 950 K (red line with filled circles) case. The corresponding almost straight lines show the initial mixture temperature.



(a)

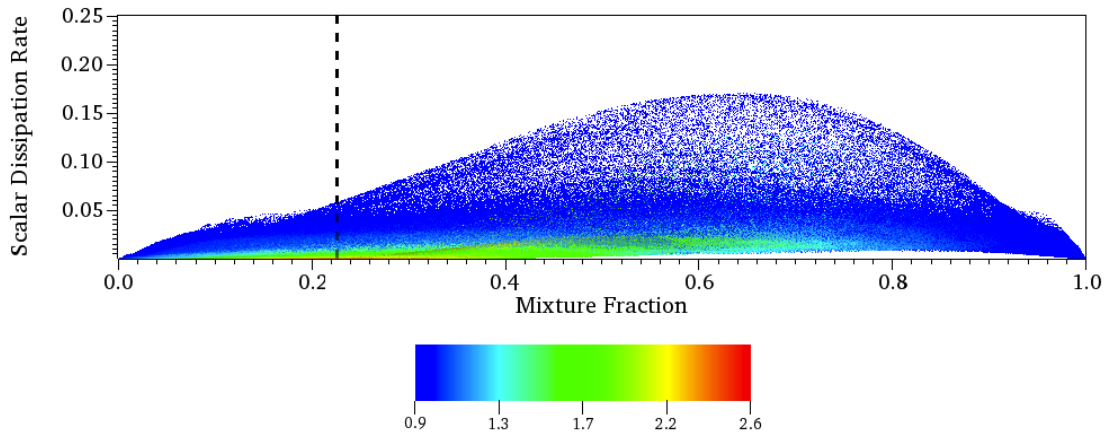


(b)

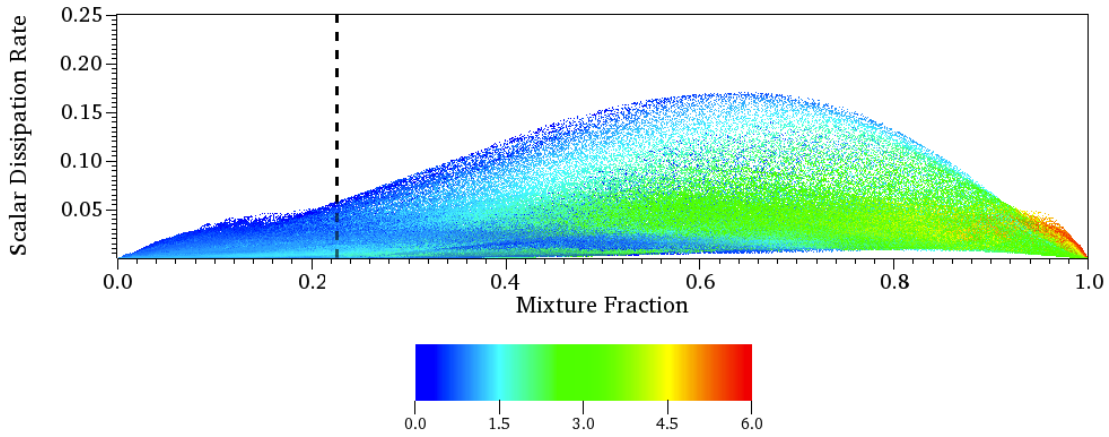


(c)

**Figure 8: Temperature distribution over a mid span wise ( $xz$ ) plane ( $y = 0$ ) for the  $T_{cf} = 930$  K case, (a)  $t=23.5$ , (b)  $t=30.1$ , (c) time average. Two mixture fraction isolines are overlaid; the most reactive ( $\xi_{MR} = 0.03$  in red) and the stoichiometric ( $\xi_{st} = 0.226$  in black).**



(a)



(b)

**Figure 9: Scatter plot of the mean mixture fraction & scalar dissipation rate colored by (a) temperature, (b) velocity magnitude for the  $T_{cf} = 930$  K case. Dashed line corresponds to the stoichiometric mixture fraction  $\xi_{st} = 0.226$ . To avoid the inert span wise region, the data is limited to  $y \in [-1 - 1]$  and the pipe region is also excluded.**

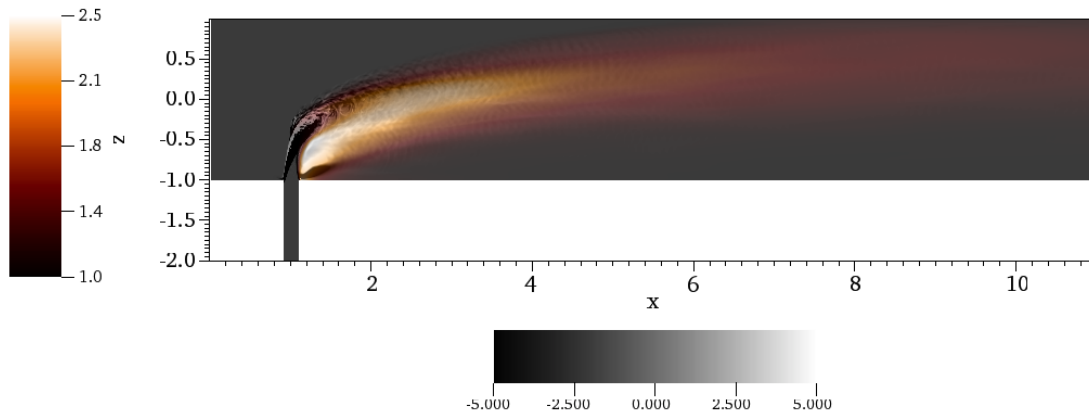


**Figure 10: The mean Takeno flame index (grey colormap) over a mid spanwise ( $xz$ ) plane overlaid on the mean temperature field (semi-transparent orange colormap). Light regions correspond to positive Takeno index (premixed flame) while dark shades represent negative values (diffusion flame).**

air efficiently into the fuel jet. Ignition occurs initially at isolated spots far downstream from the jet where the ignition delay time is minimum. Later on, strongly burning flame stabilized behind the jet in a region where the mixture fraction dissipation rate and the velocity magnitude are relatively small. It might be argued that the CVP system and the pressure variations across the jet act as an efficient local “premixer” on the downstream side of the jet. On the other hand, cross-flow fluid on the upstream side of the jet seems to be drawn into the jet mainly through interaction with the much smaller shear layer rollers.

## Acknowledgments

This research used resources of the Argonne Leadership Computing Facility at Argonne National Laboratory. This work was supported by the Office of Science of the U.S. Department of Energy under contract DE-AC02-06CH11357. The simulations were performed on the IBM Blue Gene/Q system mira of the Argonne Leadership Computing Facility (ALCF).

## References

- [1] K. Döbbeling, J. Hellat, and H. Koch. *ASME J. Eng. Gas Turbines Power*, 129 (2007) 2.
- [2] D.J. Micka and J.F. Driscoll. *Combust. Flame*, 159 (2012) 1205–1214.
- [3] A.R. Karagozian. *Prog. Energy Combust. Sci.*, 36 (2010) 531–553.
- [4] S. Bagheri, P. Schlatter, P.J. Schmid, and D.S. Henningson. *J. Fluid Mech.*, 624 (2009) 33–44.
- [5] R.W. Grout, A. Gruber, H. Kolla, P.-T. Bremer, J.C. Bennett, A. Gyulassy, and J.H. Chen. *J Fluid Mech.*, 1 (2012) 1–33.
- [6] S.H. Smith and M.G. Mungal. *J. Fluid Mech.*, 357 (1998) 83–122.
- [7] S. Muppidi and K. Mahesh. *J. Fluid Mech.*, 530 (2005) 81–100.

- [8] S. Muppidi and K. Mahesh. *J. Fluid Mech.*, 574 (2007) 59–84.
- [9] E.F. Hasselbrink and M.G. Mungal. *J. Fluid Mech.*, 443 (2001) 27–68.
- [10] J.M. Fleck, P. Griebel, A.M. Steinberg, C.M. Arndt, C. Naumann, and M. Aigner. *Proc. Combust. Inst.*, 34 (2013) 3185–3192.
- [11] R.W. Grout, A. Gruber, C.S. Yoo, and J.H. Chen. *Proc. Combust. Inst.*, 33 (2011) 1629–1637.
- [12] H. Yamashita, M. Shimada, and T. Takeno. *Proc. Combust. Inst.*, 26 (1996) 27–34.
- [13] J.W. Lottes P.F. Fischer and S.G. Kerkemeier. nek5000 Web page, 2008. <http://nek5000.mcs.anl.gov>.
- [14] M.O. Deville, P.F. Fischer, and E.H. Mund. *High-order methods for incompressible fluid flow*, Vol. 9. Cambridge University Press, 2002.
- [15] A.G. Tomboulides, J.C.Y. Lee, and S.A. Orszag. *J. Sci. Comp.*, 12 (1997) 139–167.
- [16] S.D. Cohen and A.C. Hindmarsh. *Comp. Physics*, 10 (1996) 138–143.
- [17] R.J. Kee, G. Dixon-Lewis, J. Warnatz, M.E. Coltrin, and J.A. Miller. *Sandia National Laboratories*, (1986) .
- [18] S. Muppidi and K. Mahesh. *J. Fluid Mech.*, 598 (2008) 335–360.
- [19] C.N. Markides and E. Mastorakos. *Proc. Combust. Inst.*, 30 (2005) 883–891.
- [20] E. Mastorakos. *Prog. Energy Combust. Sci.*, 35 (2009) 57–97.